Supplementary Information

Oxygen vacancies boost the efficacy of MnO_2 nanoparticles in catalyzing hydrolytic degradation of organophosphate esters: Implications for managing plastic additive pollution

Zongsheng Liang [#], Keman Liu [#], Yueyue Li, Yaqi Liu, Chuanjia Jiang[*], Tong Zhang[*], Wei Chen

College of Environmental Science and Engineering, Ministry of Education Key Laboratory of Pollution Processes and Environmental Criteria, Tianjin Key Laboratory of Environmental Remediation and Pollution Control, Nankai University, Tianjin 300350, China

* Corresponding authors: (Phone/fax) 86-22-85358169; (E-mail) jiangcj@nankai.edu.cn, zhangtong@nankai.edu.cn.

[#] These authors contributed equally to this work.

Text S1

Chemicals. The 4-nitrophenyl phosphate disodium hexahydrate (pNPP, 99.8%), 4-nitrophenol (4-NP,99%), acetonitrile (CH_3CN, 99.5%) were purchased from Aladdin Corporation (Shanghai, China). 3-(N-morpholino)-propane sulfonic acid (MOPS, 99%) and manganese acetate tetrahydrate ($Mn(CH_3COO)_2 \cdot 4H_2O$, 99.8%) were purchased from Sigma-Aldrich (USA). sodium hydroxide (NaOH, 98%), hydrochloric acid (HCl, 37%), potassium permanganate ($KMnO_4$, 99.7%) and methanol (CH_3OH, 99%) were obtained from Tianjin Chemical Reagent Co. (Tianjin, China). Ultrahigh-purity nitrogen were supplied by Tianjin Hollen Gas Co., Ltd (Tianjin, China). Deionized water (18 MΩ cm at 25 °C) from a Millipore water purification system was used throughout the experiments. All chemicals were analytical grade and used without further purification.

Text S2

Material Characterization Methods. The morphology of the samples was characterized using a field-emission scanning electron microscope (JEOL JSM-2100F, Japan) and a field-emission transmission electron microscope (JEOL JEM-2800, Japan). The crystalline phases of the materials were determined using a powder X-ray diffractometer (Ulitma IV, Rigaku, Japan). X-ray photoelectron spectroscopy (XPS) measurements were carried out on a ESCALAB 250Xi spectrometer (Thermo Scientific, U.S.A.) using a focused monochromatic Al Kα X-ray beam (1486.6 eV). Raman spectroscopy measurements were conducted on a RM2000 microscope system (Renishaw, England) using an excitation wavelength of 532 nm. Nitrogen adsorption/desorption isotherms were measured with an ASAP 2020 surface area analyzer (Thermo Fisher, Micromeritics, U.S.A.). Pyridine adsorption infrared spectroscopy (py-IR) was

performed using a Thermo Nicolet 380 FTIR spectrometer (Thermo Fisher, Massachusetts, U.S.A.), and temperature-programmed desorption of ammonia (NH_3-TPD) using a Chemisorb-2720 instrument (Thermo Fisher, Massachusetts, U.S.A.). The zeta potential of the nanoparticles in aqueous suspension was measured using a particle size analyzer (Litesizer 500, Anton Paar, Austria). Electron paramagnetic resonance (EPR) tests were performed on a Bruker ER 100d X-band spectrometer.

Text S3

Hydrolysis Experiments of pNPP. Batch experiments were carried out in 40-mL amber glass vials sealed with Teflon-lined caps to avoid potential light-induced reactions. Each vial contained 40 mL of 5.0 mM MOPS/MOPS-Na buffer solution, adjusted to various pH values (5.0, 6.0, 7.0, and 8.0), and the α-MnO_2 materials were added to achieve a surface area concentration of 25 m^2 L^{-1}. These vials were then placed on a horizontal rotary thermostatic oscillator to ensure thorough hydration and wetting for 12 h at 180 rpm and 25 ± 0.5 °C. Following this, 80 μL of a 6 g L^{-1} pNPP stock solution (dissolved in methanol) was injected, establishing an initial pNPP concentration of 12 mg L^{-1}. At predetermined intervals, 1.5 mL of samples were extracted and immediately transferred to a new glass vial containing 1.5 mL of 0.1 M NaOH, then filtrated through a 0.22-μm membrane filter for subsequent analysis. pNPP and its hydrolysis products were quantified using high-performance liquid chromatography (HPLC) equipped with a UV detector at a wavelength of 310 nm (Waters 2695e, U.S.A.). Chromatographic separation was achieved on a reversed-phase C18 column (4.6 × 150 mm, maintained at 30°C) with an isocratic elution of 40% acetonitrile and 60% water at a flow rate of 1 mL min^{-1}. Each experiment was conducted in triplicate.

Text S4

Data Analysis. The pNPP hydrolysis kinetics data were fitted to the pseudo-first-order kinetic model:

$$C_t/C_0 = \exp(-k_{obs}\, t) \qquad \text{(S1)}$$

where C_0 (mg L^{-1}) is the initial pNPP concentration, C_t (mg L^{-1}) is the pNPP concentration at a given time t (h), and k_{obs} (h^{-1}) is the apparent pseudo-first-order rate constant.

The Langmuir-Hinshelwood model (equation S2) was employed to fit the kinetics data with different initial concentrations (C_0), and the adsorption coefficient (K_L, L mg^{-1}) and the surface reaction rate constant (k_r, mg L^{-1} h^{-1}) of pNPP on the MnO_2 were obtained from the linearized equation (S3).[1]

$$r_0 = \frac{k_r \cdot K_L \cdot C_0}{1 + K_L \cdot C_0} \qquad \text{(S2)}$$

$$\frac{1}{r_0} = \frac{1}{k_r} + \frac{1}{k_r \cdot K_L \cdot C_0} \qquad \text{(S3)}$$

where where r_0 (mg L^{-1} h^{-1}) is the initial reaction rate, which was calculated according to equation S4:

$$r_0 = k_{obs}\, C_0 \qquad \text{(S4)}$$

Text S5

In Situ Attenuated Total Reflectance Fourier Transform Infrared Spectra (in situ ATR-FTIR) Measurements of pNPP Adsorption. In situ ATR-FTIR spectra were collected using a HATRPlus accessory installed in a Nicolet 8700 FTIR spectrometer (Thermo, U.S.A.) equipped with a purge gas generator and a liquid-nitrogen-cooled mercury cadmium telluride detector. The

ATR flow cell houses a 45° ZnSe crystal as the internal reflection element measuring 80 × 10 × 4 mm. α-MnO_2 films were directly deposited onto the ZnSe crystal from slurries containing a known amount of powder in a water/ethanol mixture. Briefly, 500 μL of a 2 g L^{-1} MnO_2 suspension was evenly spread on the ZnSe crystal and left to be air-dried overnight to form a uniform film. This film was gently rinsed with ultrapure water to flush out the loosely adhered particles and impurities, followed by preliminary equilibration with ultrapure water adjusted to pH 6.0 using 0.1 mol L^{-1} HCl or NaOH, at a flow rate of 1.0 mL min^{-1} until there was no further change observed in the spectra. All spectra were acquired with 256 scans across a wavenumber range of 800−1500 cm^{-1} with a resolution of 4 cm^{-1}. A background spectrum was recorded to account for the absorbance of the ZnSe crystal, the α-MnO_2 film, and ultrapure water, with all subsequent spectra obtained as ratios against this background. The solution flowing over the film was then switched to 100 mg L^{-1} pNPP solution, adjusted to the same pH. Preliminary experiments on the bare ZnSe crystal showed that the contributions from dissolved pNPP (100 mg L^{-1}) were negligible in the FTIR spectrum.

Text S6

Theoretical Calculation. The density functional theory (DFT) calculations were performed using the Vienna Ab initio Simulation Package (VASP 5.4.4). To minimize periodic boundary effects, a vacuum layer of 15 Å was added in the perpendicular direction. The core-electronic interactions were treated with wave using the generalized gradient approximation (GGA) of the electronic exchange-correlation functional (Perdew-Burke-Ernzerhof, PBE). A Hubbard U correction was applied with specific parameters set for Mn (1.6), LDAUU (2.8), and LDAUJ (1.2).[2] K-points in the first Brillouin zone were sampled using a (2 × 1 × 1) Monkhorst-Pack grid,

with the plane wave cutoff energy set to 420 eV. Convergence criteria were established at 10^{-6} eV for energy and 0.05 eV $Å^{-1}$ for forces. The lattice constants were held constant, allowing only internal atomic positions to relax; the bottom eight layers retained their positions, while the upper layers were allowed to relax. The DFT-D3 method was used to account for van der Waals forces and model interactions involving hydrogen bonds between water molecules, pNPP, and the material surface. Calculations used the predominant pNPP and $pNPP^{2-}$ species (the total number of valence electrons for pNPP was increased by 2) at low and high pH, respectively. The adsorption energies (E_{ads}) were calculated according to eqation S5:

$$E_{ads} = E_{slab+H2O+pNPP} - E_{slab+H2O} - E_{pNPP} \qquad (S5)$$

where $E_{slab+H2O+pNPP}$ is the total energy of the optimized slab model with H_2O molecules and the pNPP complex, $E_{slab+H2O}$ represents the energy of the slab model with H_2O molecules before pNPP adsorption, and E_{pNPP} is the initial energy of the pNPP alone. This approach offers a detailed molecular-level insight into the adsorption processes.

Table S1. Specific surface area and pore volume of α-MnO_2-N200, α-MnO_2, and α-MnO_2-O200.

Sample	Specific surface area (m^2 g^{-1})	Pore volume (cm^3 g^{-1})
α-MnO_2-N200	129.3 ± 8.3	0.31
α-MnO_2	103.1 ± 9.6	0.22
α-MnO_2-O200	91.6 ± 6.7	0.25

Table S2. XPS fitting parameters of α-MnO_2-N200, α-MnO_2, and α-MnO_2-O200.

Sample	Orbitals	Binding energy (eV)	FWHM (eV)	Area (CPS eV^{-1})	Assignment	Atomic (%)
α-MnO_2-N200	Mn $2p_{3/2}$	640.7 ± 0.1	1.4 ± 0.1	9403.8 ± 11.2	Mn(II)	15.4 ± 0.2
	Mn $2p_{1/2}$	652.4 ± 0.1	1.4 ± 0.1	4694.9 ± 5.5		
	Mn $2p_{3/2}$	641.8 ± 0.1	1.5 ± 0.1	28065.5 ± 28.6	Mn(III)	45.9 ± 0.1
	Mn $2p_{1/2}$	653.3 ± 0.1	1.5 ± 0.1	14011.7 ± 13.1		
	Mn $2p_{3/2}$	643.0 ± 0.1	2.0 ± 0.1	23702.5 ± 37.5	Mn(IV)	38.8 ± 0.1
	Mn $2p_{1/2}$	654.5 ± 0.1	2.0 ± 0.1	11833.5 ± 15.9		
α-MnO_2	Mn $2p_{3/2}$	640.6 ± 0.1	1.4 ± 0.1	9439.5 ± 23.4	Mn(II)	12.2 ± 0.2
	Mn $2p_{1/2}$	652.4 ± 0.1	1.4 ± 0.1	4155.7 ± 11.2		
	Mn $2p_{3/2}$	641.8 ± 0.1	1.5 ± 0.1	33472.5 ± 32.3	Mn(III)	43.1 ± 0.1
	Mn $2p_{1/2}$	653.3 ± 0.1	1.5 ± 0.1	17463.2 ± 17.6		
	Mn $2p_{3/2}$	643.0 ± 0.1	2.0 ± 0.1	34718.6 ± 39.5	Mn(IV)	44.7 ± 0.1
	Mn $2p_{1/2}$	654.6 ± 0.1	2.0 ± 0.1	18905.6 ± 19.1		
α-MnO_2-O200	Mn $2p_{3/2}$	640.6 ± 0.1	1.4 ± 0.1	8323.8 ± 12.6	Mn(II)	10.3 ± 0.1
	Mn $2p_{1/2}$	652.4 ± 0.1	1.4 ± 0.1	4155.7 ± 6.6		
	Mn $2p_{3/2}$	641.8 ± 0.1	1.5 ± 0.1	34978.7 ± 27.4	Mn(III)	43.1 ± 0.1
	Mn $2p_{1/2}$	653.3 ± 0.1	1.5 ± 0.1	17463.2 ± 14.9		
	Mn $2p_{3/2}$	643.1 ± 0.1	2.0 ± 0.1	37868.0 ± 36.1	Mn(IV)	46.7 ± 0.1
	Mn $2p_{1/2}$	654.4 ± 0.1	2.0 ± 0.1	18905.6 ± 20.3		

Notes: FWHM is the full width at half maximum intensity.

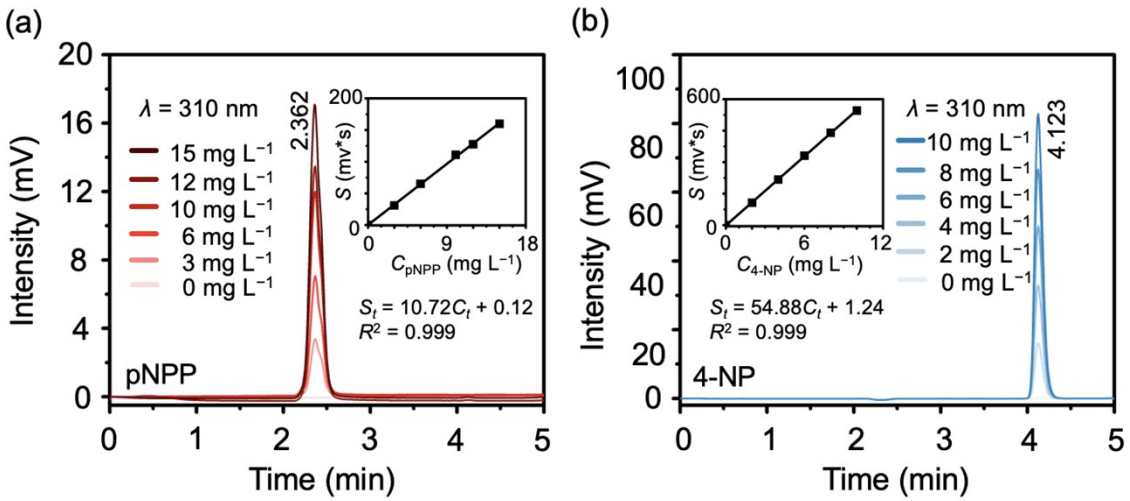

Figure S1. HPLC spectra for the analysis of (a) pNPP and (b) 4-NP at various concentrations, ranging from 0 to 15 mg L^{-1} for pNPP and from 0 to 10 mg L^{-1} for 4-NP. The insets show the standard calibration curves with linear fitting results for pNPP and 4-NP, respectively.

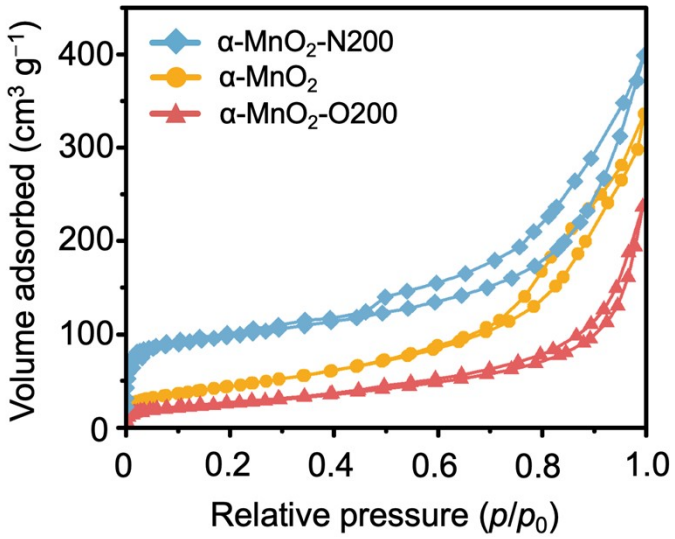

Figure S2. Nitrogen adsorption-desorption isotherms of α-MnO_2-N200, α-MnO_2, and α-MnO_2-O200.

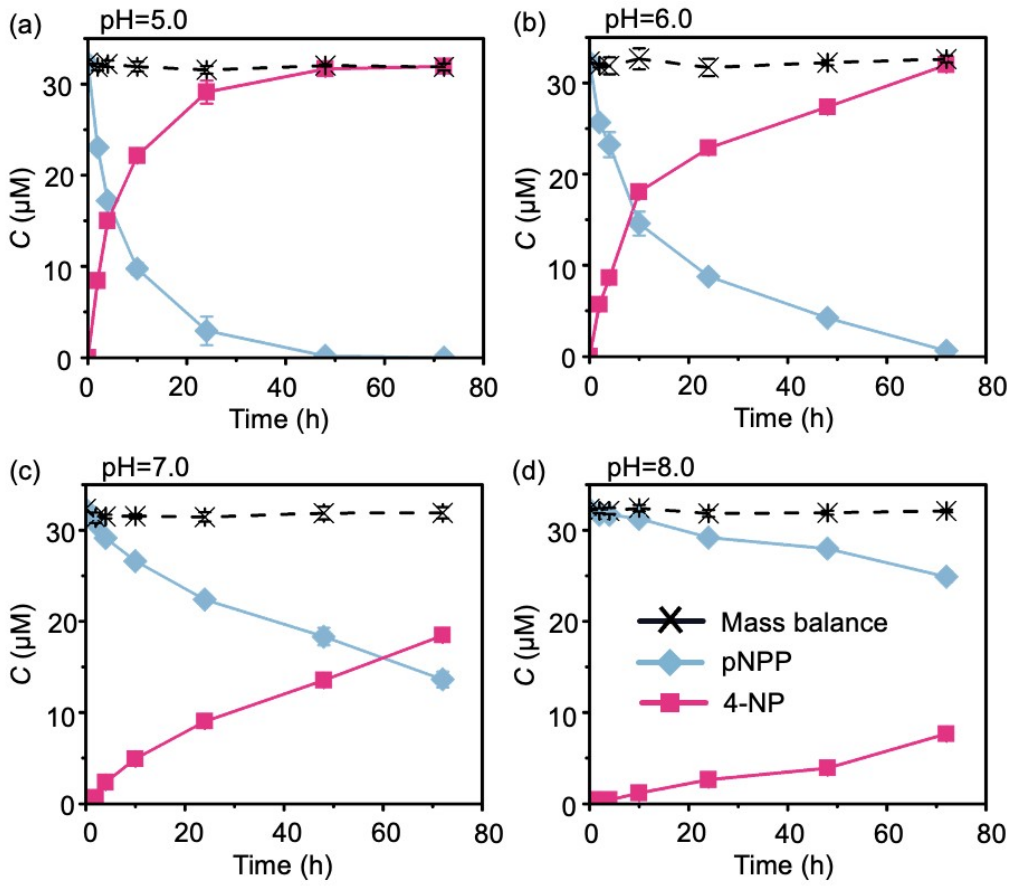

Figure S3. Variations in pNPP and 4-NP concentrations during pNPP hydrolysis experiments in aqueous suspensions of α-MnO_2-N200 at different pH values: (a) pH = 5.0, (b) pH = 6.0, (c) pH = 7.0, and (d) pH = 8.0. Error bars represent standard deviations of triplicate samples. Reaction condition: 5 mM MOPS/MOPS-Na buffer, surface area concentration of materials = 25 m^2 L^{-1}, initial pNPP concentration = 12 mg L^{-1}, 25 °C.

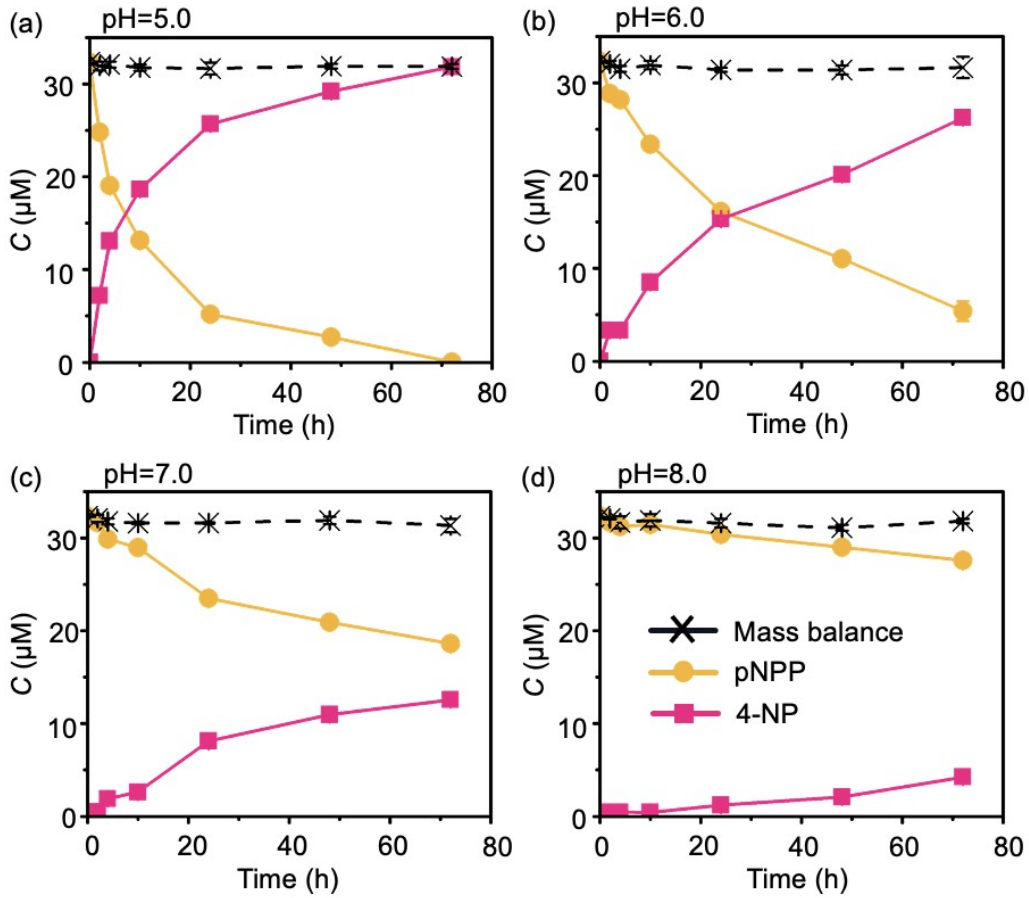

Figure S4. Variations in pNPP and 4-NP concentrations during pNPP hydrolysis experiments in aqueous suspensions of α-MnO_2 at different pH values: (a) pH = 5.0, (b) pH = 6.0, (c) pH = 7.0, and (d) pH = 8.0. Error bars represent standard deviations of triplicate samples. Reaction condition: 5 mM MOPS/MOPS-Na buffer, surface area concentration of materials = 25 m^2 L^{-1}, initial pNPP concentration = 12 mg L^{-1}, 25 °C.

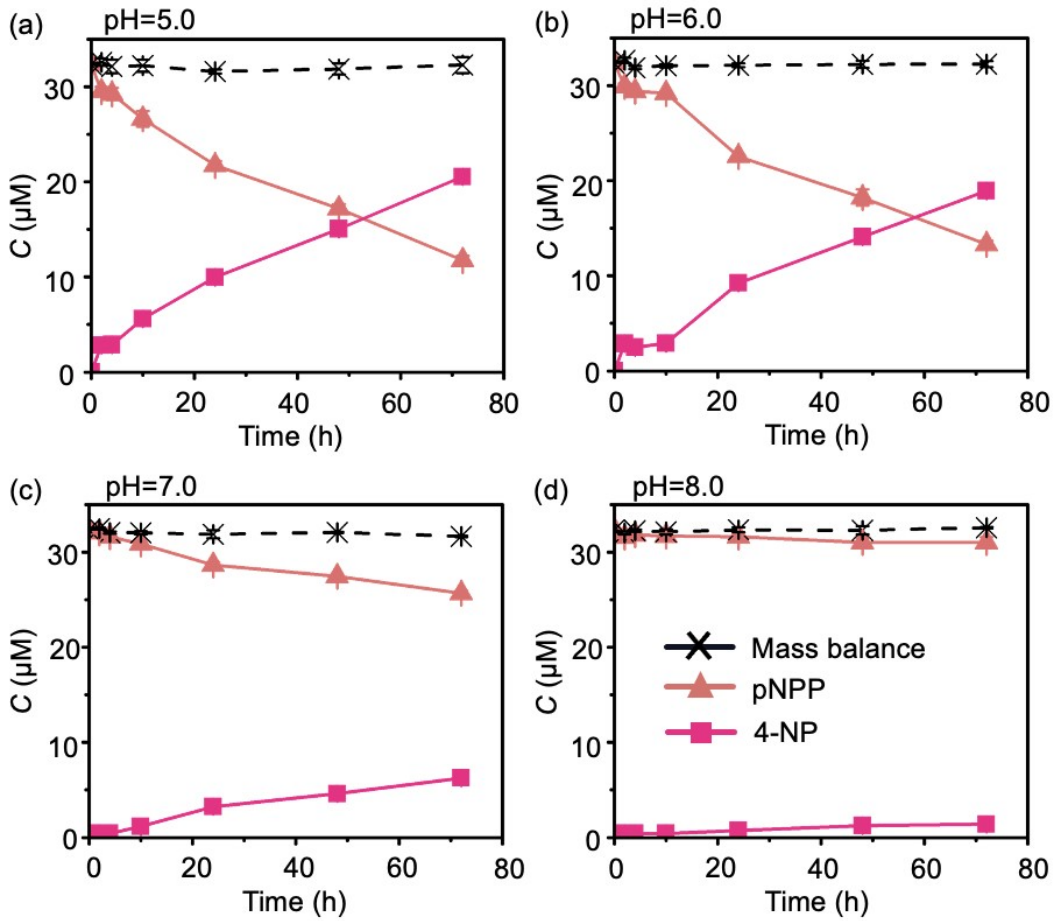

Figure S5. Variations in pNPP and 4-NP concentrations during pNPP hydrolysis experiments in aqueous suspensions of α-MnO_2-N200 at different pH values: (a) pH = 5.0, (b) pH = 6.0, (c) pH = 7.0, and (d) pH = 8.0. Error bars represent standard deviations of triplicate samples. Reaction condition: 5 mM MOPS/MOPS-Na buffer, surface area concentration of materials = 25 m^2 L^{-1}, initial pNPP concentration = 12 mg L^{-1}, 25 °C.

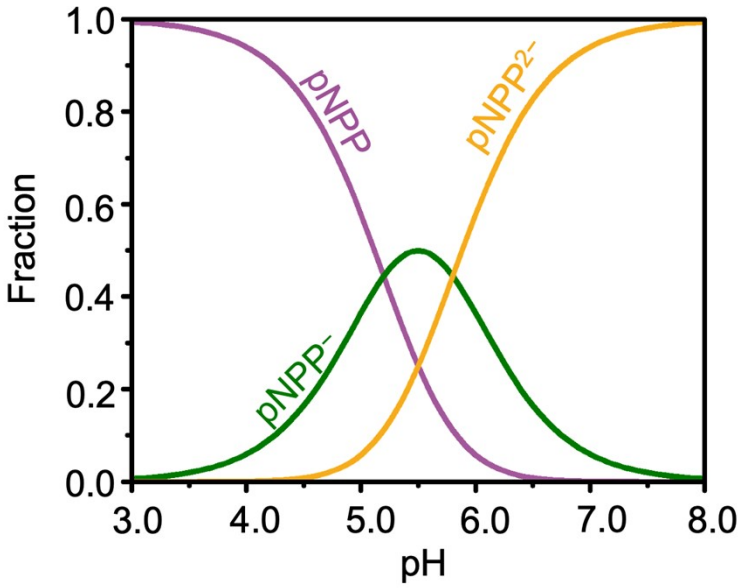

Figure S6. Speciation of pNPP in aqueous solution with an ionic strength of 5 mM at 25 °C. The acid dissociation constants of pNPP, pK_{a1} and pK_{a2}, are 5.2 and 5.8.[3] The activity coefficients for the deprotonated species $pNPP^{-}$ and $pNPP^{2-}$ were estimated to be 0.93 and 0.74, respectively, according to the Davies Equation.

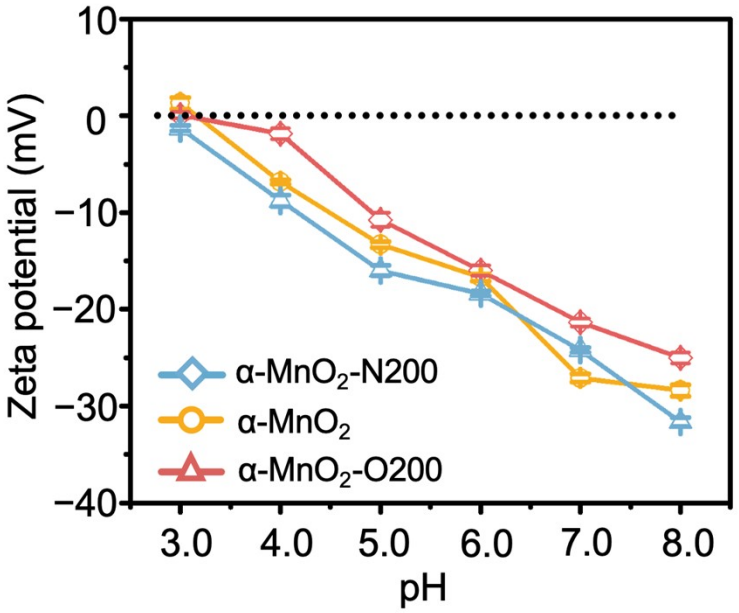

Figure S7. Zeta potential of α-MnO_2-N200, α-MnO_2, and α-MnO_2-O200 at different pH values.

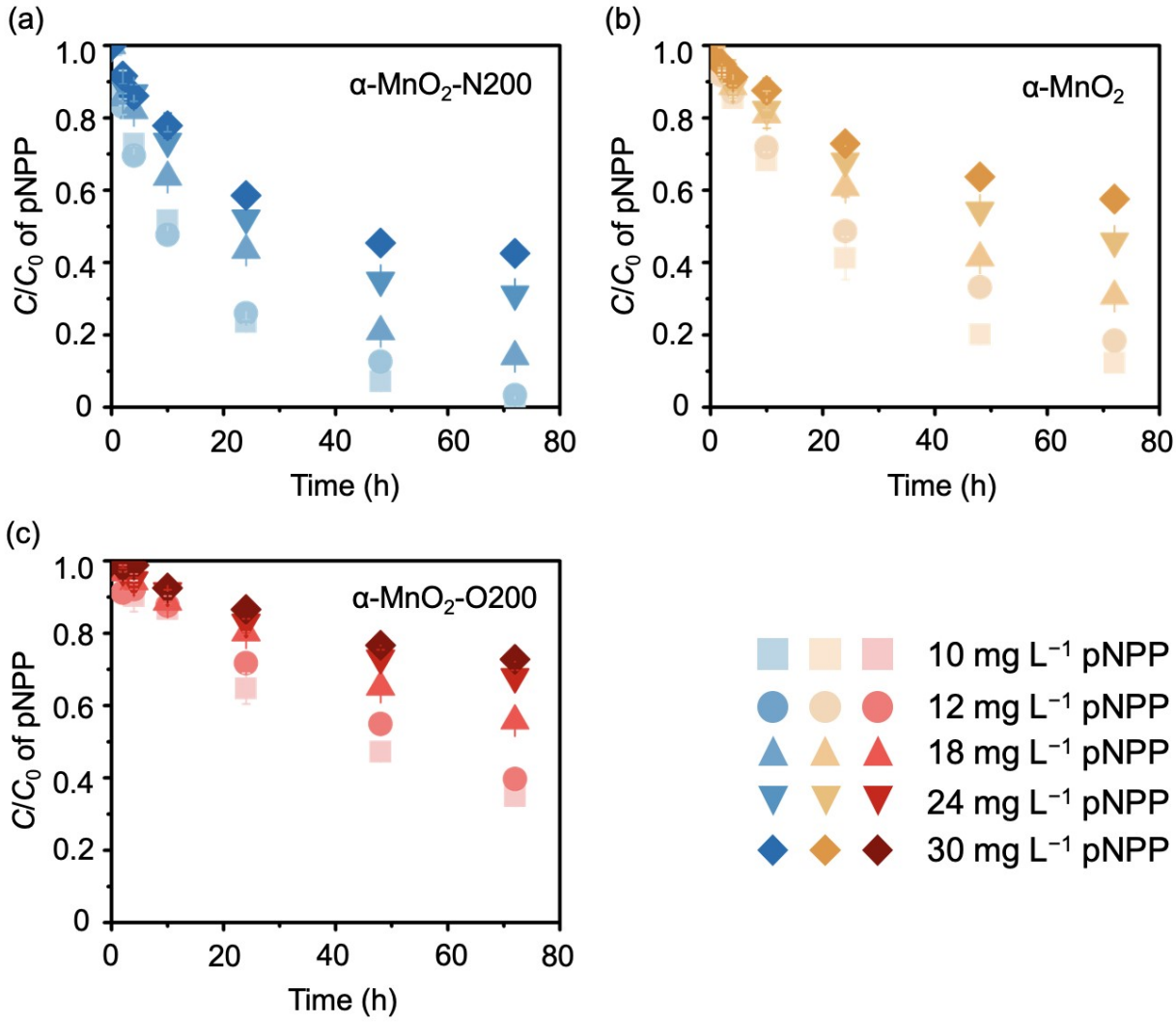

Figure S8. Catalytic hydrolysis kinetics of pNPP with different initial concentrations by (a) α-MnO_2-N200, (b) α-MnO_2, and (c) α-MnO_2-O200 at pH 6.0.

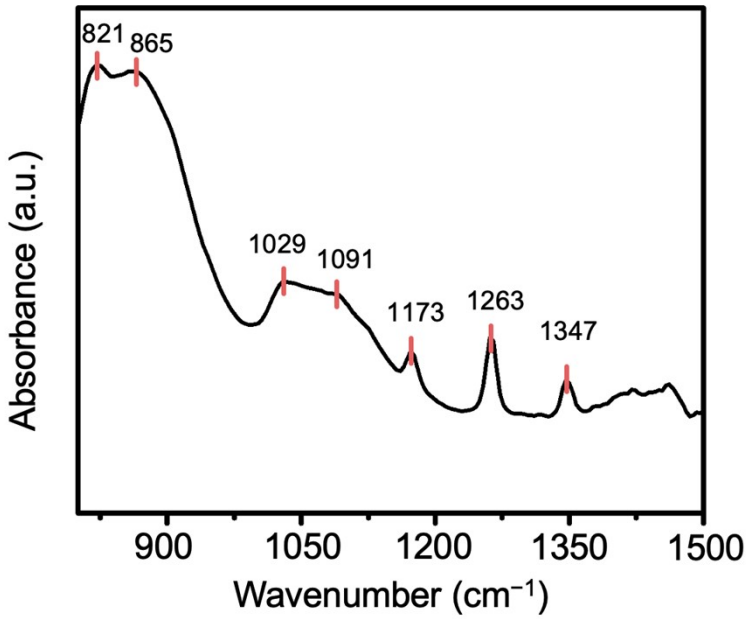

Figure S9. ATR-FTIR spectrum of pNPP in aqueous solution at pH 6.0.

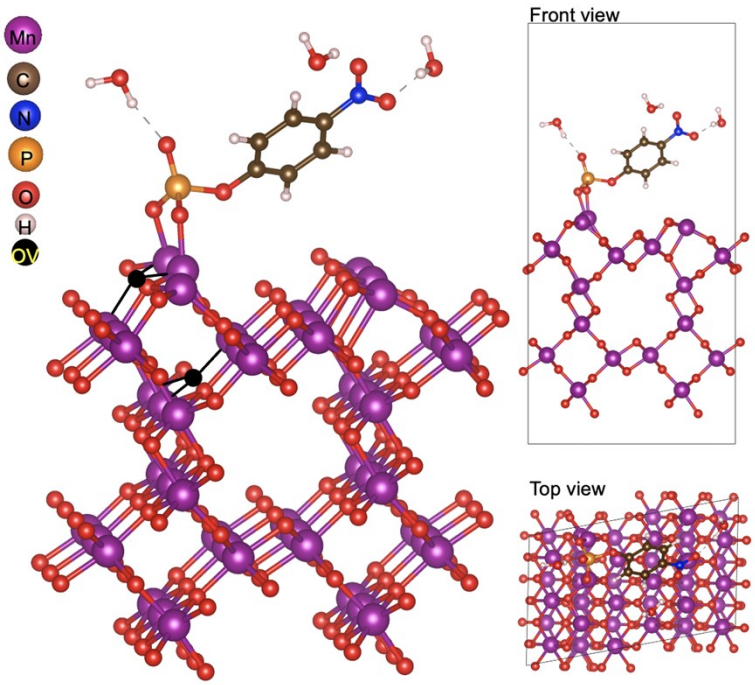

Figure S10. Structural models after the adsorption of pNPP on α-MnO_2 with OVs (α-MnO_2-OVs) via the $-NO_2$ group.

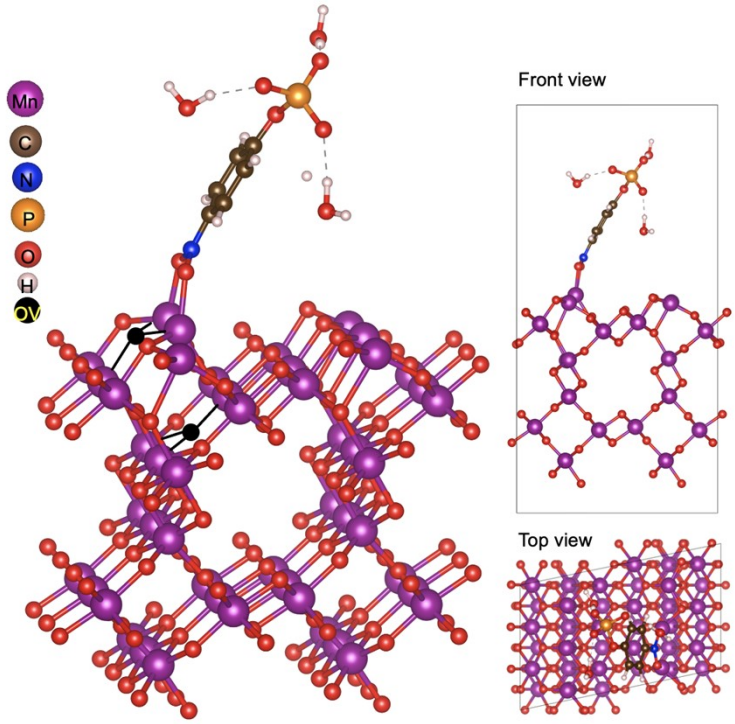

Figure S11. Structural models after the adsorption of pNPP on α-MnO_2-OVs via the $-PO_4$ group.

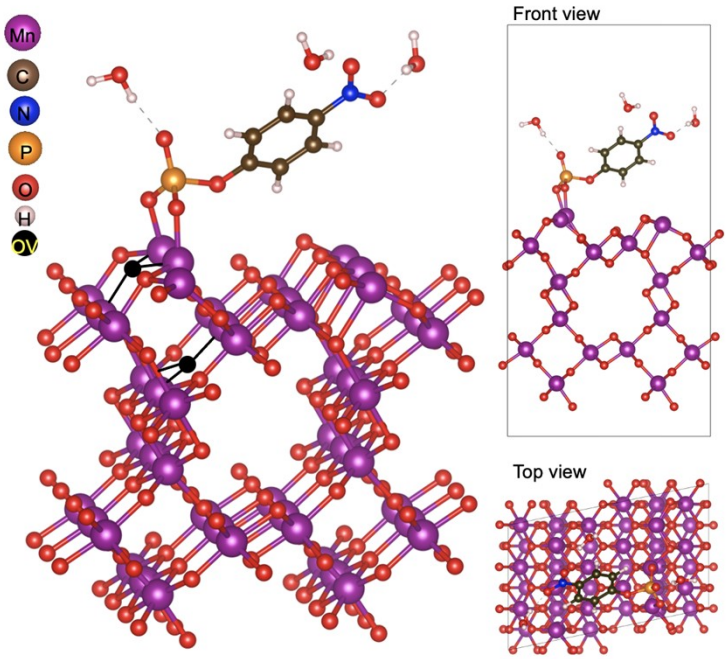

Figure S12. Structural models after the adsorption of $pNPP^{2-}$ on α-MnO_2-OVs via the $-PO_4$ group.

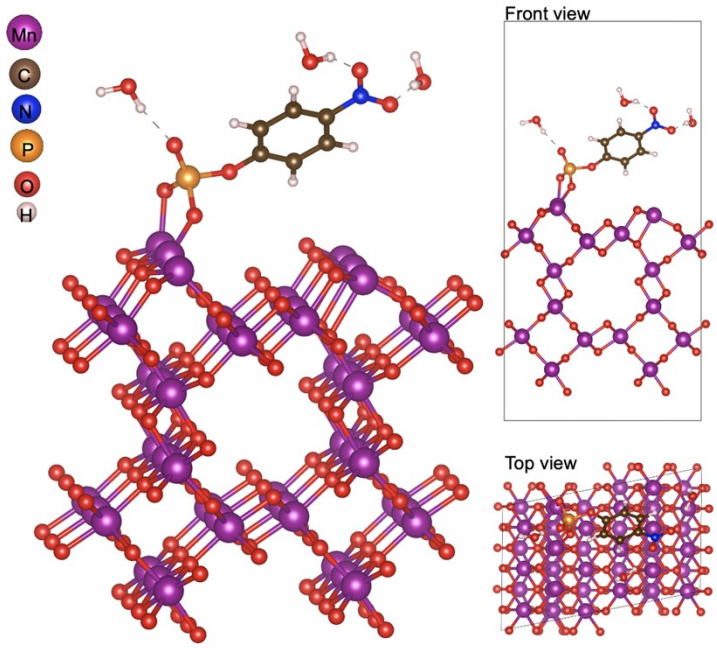

Figure S13. Structural models after the adsorption of pNPP on α-MnO_2 via the $-NO_2$ group.

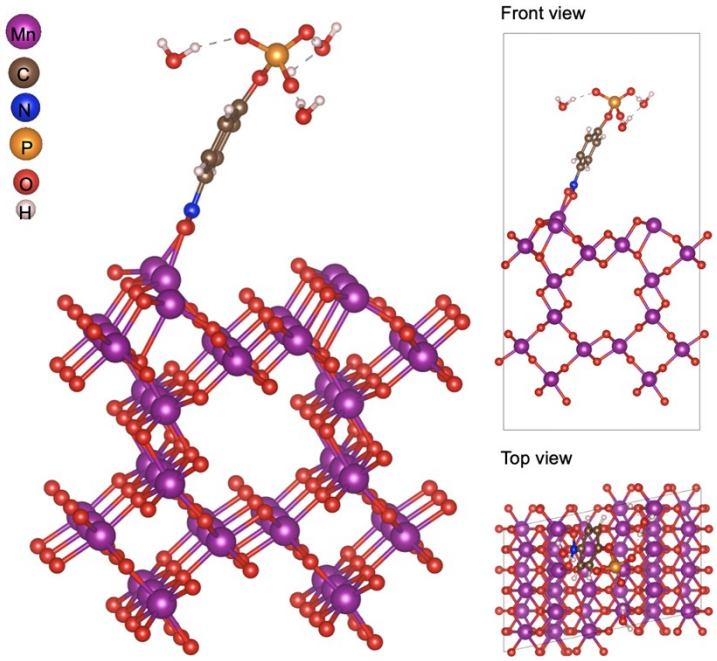

Figure S14. Structural models after the adsorption of pNPP on α-MnO_2 via the $-PO_4$ group.

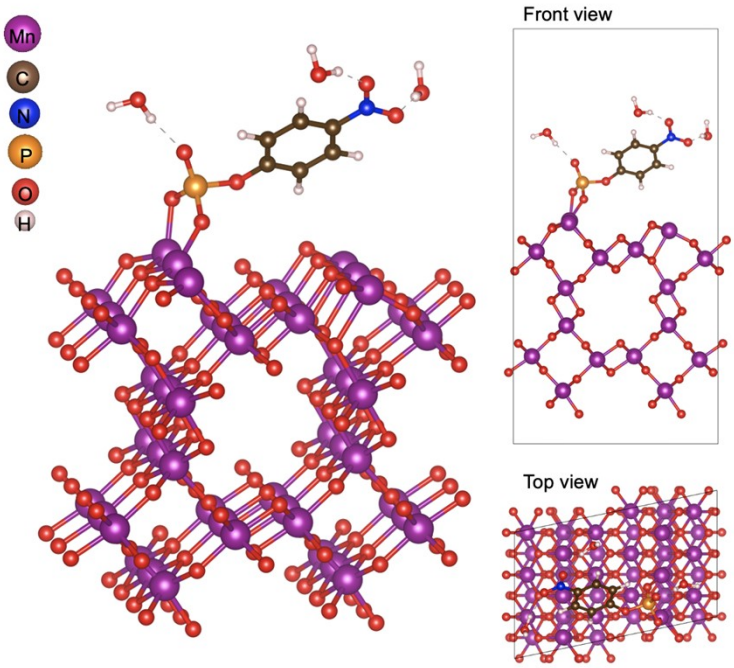

Figure S15. Structural models after the adsorption of $pNPP^{2-}$ on α-MnO_2 via the $-PO_4$ group.

References

1. K. V. Kumar, K. Porkodi and F. Rocha, Langmuir–Hinshelwood kinetics – A theoretical study, *Catalysis Communications*, 2008, **9**, 82–84.

2. E. Cockayne and L. Li, First-principles DFT+U studies of the atomic, electronic, and magnetic structure of α-MnO_2 (cryptomelane), *Chem. Phys. Lett.*, 2012, **544**, 53–58.

3. M. Li, R. L. Harbron, J. V. M. Weaver, B. P. Binks and S. Mann, Electrostatically gated membrane permeability in inorganic protocells, *Nat. Chem.*, 2013, **5**, 529–536.